

Hierarchical Assembly and Enhanced Lithium Storage Properties of 3D SnO₂/PC Hybrids

Yuzhen Sun, Yumei Chen, Xiaowei Yang, Yuxiang Zuo, Zhiyuan Zhao* and Bing Huang*

Institute of New Energy on Chemical Storage and Power Sources, College of Applied Chemistry and Environmental Engineering, Yancheng Teachers University, Jiangsu, Yancheng 224000, China.

*E-mail: xiaoweiayang215@126.com, zhiyuan.zhao@rcclab.com

Received: 27 July 2020 / Accepted: 15 September 2020 / Published: 10 October 2020

Ultrasmall SnO₂ nanoparticles (~ 3 nm in diameter) confined in three dimensional hierarchical porous carbon (3D SnO₂/PC) were successfully prepared using a simple method in this work. The 3D SnO₂/PC has almost monodispersion of the SnO₂ nanoparticles with 73 wt% load. The 3D SnO₂/PC exhibits excellent performance with high rate capability and significant cycle stability. At 0.1 A /g in the 100th cycle, the reversible specific capacity is 1374 mAh/g. These outstanding characteristics are desirable and make 3D SnO₂/PC a promising anode material for LIBs.

Keywords: 3D porous carbon; Tin dioxide; Anode; Lithium ion battery

1. INTRODUCTION

Lithium-ion batteries (LIBs) have fascinated more and more interest recently. In the industrial sector, graphite is the first commercially available LIBs anode material. However, its low theoretical capacity (372 mAh/g) and poor rate capability are not conducive to the development of high-performance LIBs [1, 2]. Therefore, much effort is paid to develop new anode materials with a variety of nanostructures and configurations to meet the high performance requirements rechargeable LIBs [1, 2]. Among many anode materials, tin dioxide (SnO₂) is one of the most studied materials due to its high theoretical capacity (782 mAh/g), non-toxic and cheap features [3-5]. However, the intense volume expansion/shrinkage and low conductivity of SnO₂ lead to poor recyclability and rate capability [6, 7]. To avoid similar poor performance, scientific research personnel construct anode materials in different ways. One tactic is the fabrication of nano-structures to buffer the volume increase. Another way is the integration of SnO₂ with the carbon substrates [1]. Graphene-based SnO₂ composites have been investigated extensively [5, 8-16]. Nevertheless, the most graphene substrates were made from graphene oxide (GO) or reduced graphene oxide (rGO) precursor, which could lead to

the formation of a very thick solid electrolyte interphase during cycling. Meanwhile, the volume of SnO₂ nanoparticles on the graphene expands and shrinks dramatically [17, 18].

3D porous carbon (PC), due to its large specific surface area, abundant pores and excellent specific conductance, is good for the dispersion of SnO₂ nanoparticles, thereby their active sites can be fully utilized [19-24]. The porous structure can accelerate the electron transport and benefit to improve electrochemical performance. Used as electrode, 3D PC-SnO₂ presents excellent survival rate [19-21].

Herein, we exploit 3D SnO₂/PC with uniform structures as well as good SnO₂ dispersion. The prepared 3D SnO₂/PC exhibits super specific capacity (1499 mAh/g), excellent rate capability, and high reversibility (92% retention after 100 cycles), which owe to the combined action of 3D porous structure, electronic conductive network and SnO₂ nanoparticles, showing great potential prospects as LIBs electrode materials.

2. EXPERIMENTAL METHOD

2.1. Synthesis of 3D porous MgO whiskers

Typically, 100 mL 1 mol/L Na₂CO₃ solution and 100 ml 1 mol/L MgCl₂ solution were added into a four necked glass flask and kept for 0.5 h under mechanical stirring of 300 rpm at 80 °C. After cooling, the resulting white sediment was filtrated out and dried in an oven at 80 °C. Then the product was calcined at 650 °C to remove crystal water and CO₂ to finally form the 3D porous MgO whiskers.

2.2. Synthesis of 3D PC

In a typical experiment, first, 10 g 3D porous MgO whisker was added into a pitch solution (1 g pitch/30 mL toluene) with violent agitation. After drying, the as-obtained pitch/MgO mixture was heated at 700 °C for 60 min protected by Ar. After purified the 3D PC was obtained.

2.3. Synthesis of 3D SnO₂/PC composites

Typically, 45 mg SnCl₂·2H₂O, 16.5 mg 3D PC and 20 mL water were homogeneous mixing. After hydrothermal reaction (200 °C for 10 h), the 3D SnO₂/PC was obtained.

2.4. Characterization

The as-synthesized materials were characterized by SEM (Quanta 200F, FEI, Holand), TEM (F20), XRD (Bruker D8 Advance) and XPS (PHI Quantera Scanning X-ray Microprobe). The N₂ adsorption-desorption measurements with BET model on a JW-BK222 instrument.

2.5. Electrochemical tests

CR2025 coin-type cells were used for evaluation at room temperature. The test voltage range is from 0.01 V to 3.0 V. A slurry containing 70% carbon materials, 10% acetylene black and 20% polyvinylidene fluoride (7:1:1) was coated on copper foils to prepare the working electrodes. The

galvanostatic charge-discharge (GCD) cycles were tested at 25 °C from 0.1 to 1 A/g. The cyclic voltammetry (CV) measurement was tested at 0.1 mV/s performed on the electrochemical workstation (CHI660E). The test condition of AC impedance spectrum is from 100 kHz to 0.01 Hz.

3. RESULTS AND DISCUSSION

3.1 SEM and TEM analysis

The 3D SnO₂/PC composites were synthesized by friendly hydrothermal method. As shown in Fig. 1a, MgCO₃·3H₂O whiskers with ~13 μm in length and ~0.8 μm in diameter have a smooth surface before calcination. After calcination at 650 °C, abundant pores can be observed inside and outside the 3D MgO whiskers (Fig. 1b). The synthesis process for 3D PC is illustrated in scheme 1 using the calcined 3D MgO whiskers as templates.

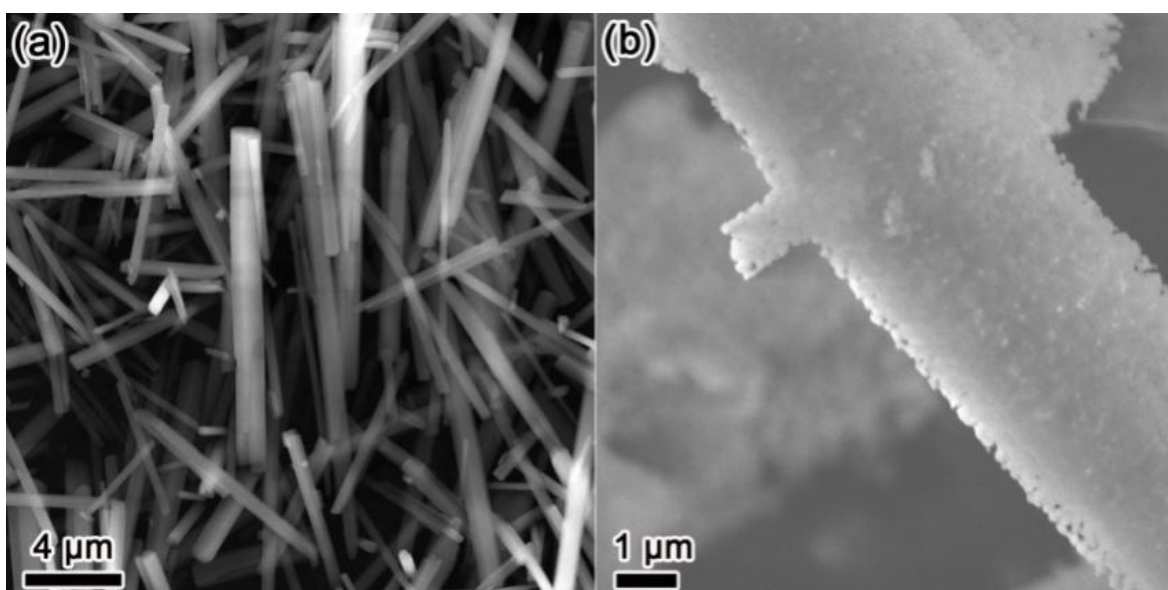
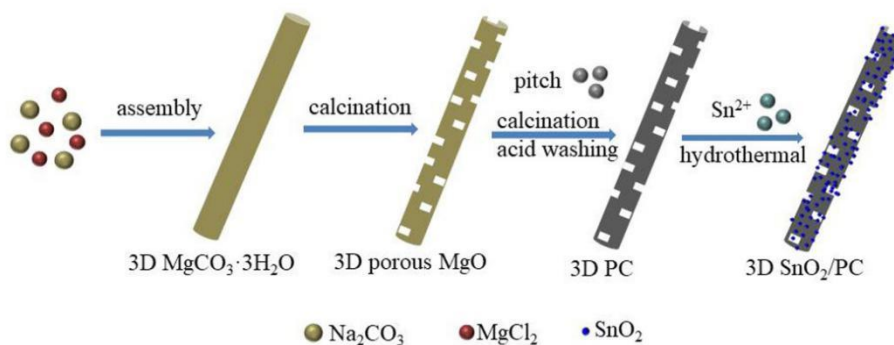


Figure 1. SEM images of MgCO₃·3H₂O whiskers (a) and 3D porous MgO whiskers after calcination at 650 °C (b).



Scheme 1. Synthetic process of 3D PC and 3D SnO₂/PC

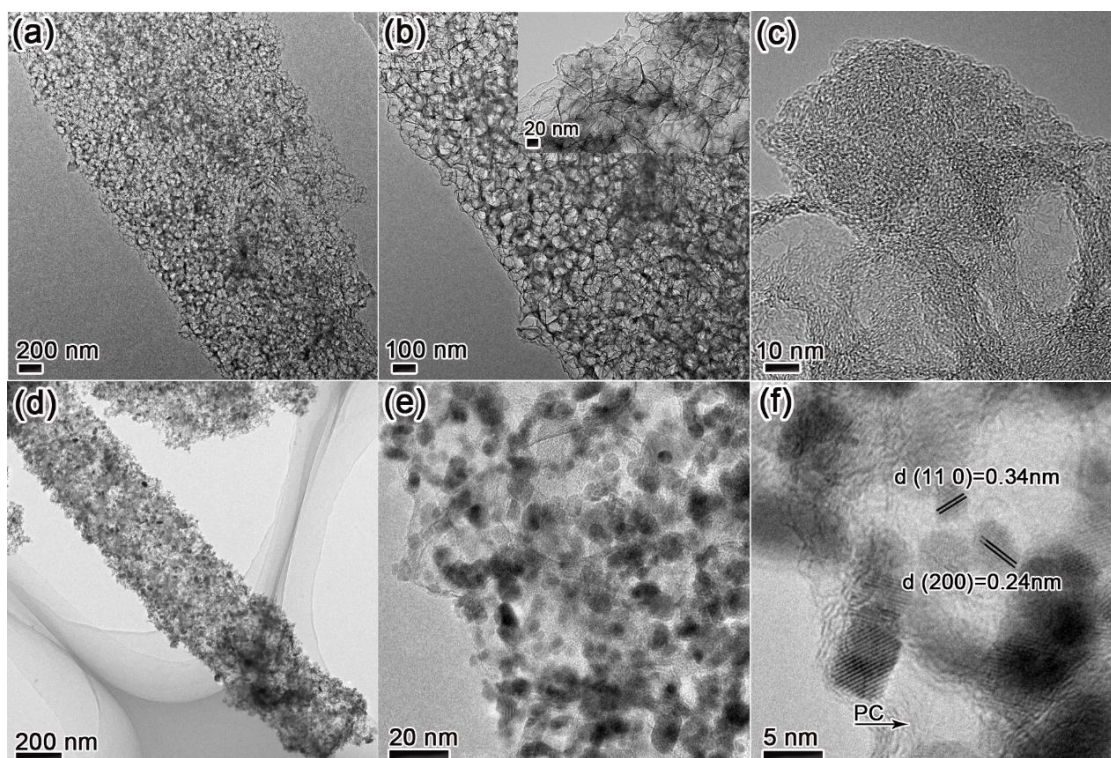


Figure 2. TEM picture of 3D PC (a, b, c) and 3D SnO₂/PC (d, e, f), the inset of (b) shows the enlarged TEM picture of PC.

The different magnified TEM images of 3D PC after removing MgO whiskers by acidic washing are shown in Fig. 2 a, b & c, illustrating a unique 3D interconnected porous structure. Such abundant micropores and mesopores are in favour of the ion storage and transport. And as a support of metal oxide, the 3D PC would be able to easily form fine metal oxide nanostructures with uniform surface distribution [25].

The synthesis process of the 3D SnO₂/PC composite was illustrated in Scheme 1. From Fig. 2d the 3D PC is uniformly covered by the ultrasmall SnO₂ nanoparticles. The morphology of 3D SnO₂/PC is similar to that of 3D PC, suggesting that there is no change for the overall morphology after the introduction of SnO₂. The 3D PC facilitates the diffusion of the liquid electrolyte and increases the electronic conductivity, which is conducive to the realization of high speed energy [26-28]. For 3D SnO₂/PC nanocomposite, SnO₂ nanoparticles adhere to 3D PC and being separated spatially by the carbon skeleton avoiding accumulation at the same time, which helps to improve cycling performance [26, 29]. As is shown in Fig. 2e, SnO₂ nanoparticles (~ 3 nm in diameter) homogeneously distributed. The HR-TEM image (Fig. 2f) clearly displayed the monodispersed SnO₂ nanoparticles on 3D PC. The clear lattice fringe exhibits planar spacing of 0.24 nm and 0.34 nm respectively, which is well consistent with SnO₂ (200, 110) plane (PDF No.41-1445) [25]. The subsize and good dispersibility of SnO₂ particles can increase the specific surface area, buffering particle changes, helpful to improve performance.

3.2 X-ray diffraction, XPS spectroscopy, TG and Porosity analysis

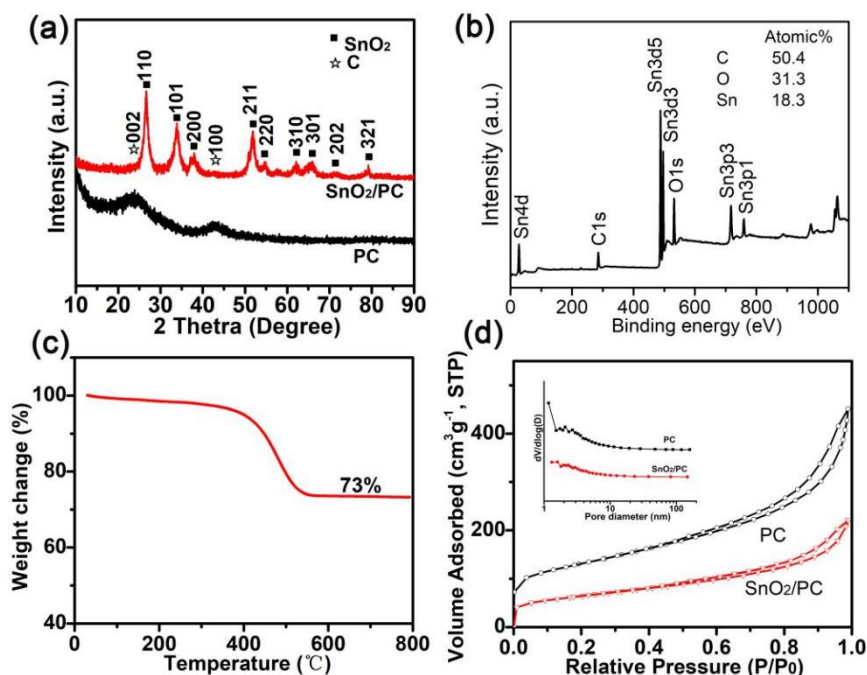


Figure 3. (a) XRD pattern of SnO₂/PC and PC. (b) XPS spectra, (c) TG analysis (O₂ atmosphere) for SnO₂/PC. (d) N₂ adsorption-desorption isotherm at 77 K (inset the corresponding PSD).

The strong diffraction peaks in SnO₂/PC (Fig. 3a) indicate the tetragonal crystal of SnO₂ (PDF No. 41-1445) [1, 25, 26, 30]. There are no obvious carbon patterns in PC, because the carbon (002) diffraction peak overlaps the SnO₂ (110) diffraction peak and PC strength is relatively weak compared to SnO₂. The average SnO₂ particle size is ~ 3.2 nm (calculated by Scherrer formula) consistent with TEM analysis. Fig. 3b shows the XPS spectra to investigate the composites of SnO₂/PC. C (50.4 atom%), O (31.3 atom%) and Sn (18.3 atom%) can be detected, confirming that SnO₂ is successful formation. Fig. 3c shows the TGA for SnO₂/PC measured in the O₂ atmosphere. From the TG curve, SnO₂/PC suffers a 24% weight loss from 280 to 800. The weight in loss is due to the combustion of PC to form CO₂. The TG curve manifests that the percentage composition of SnO₂ is ~73%, higher than SnO₂-G composite (60%) [29].

Table 1. Physical characteristics of 3D PC and 3D SnO₂/PC composites

	BET SSA	Pore volume	Pore size
Samples	(m ² /g)	(m ³ /g)	(nm)
PC	452.01	0.70	7.40
SnO ₂ /PC	224.83	0.34	7.02

It is clear in Fig. 3d that the N_2 adsorption-desorption isotherm (type III, H3 hysteresis loop at 0.55–0.98 (P/P₀)) indicates abundant mesopores exists [31]. It also can be seen that there is an uptake at a lower relative pressure (P/P₀ < 0.05) indicating that there are more micropores in PC and SnO₂/PC. Since the SnO₂ nanoparticles are confined in mesopores of PC, the BET specific surface area (SSA) and pore volume of the PC (452.01 m²/g, 0.70 m³/g) is higher than those of the SnO₂/PC (224.83 m²/g, 0.34 m³/g) (Table 1). The pore size distributions are focus on 2-5 nm and 1.0-1.5 nm for mesopores and micropores respectively (Fig. 3d). Abundant micro/mesopores facilitate the permeability of electrolytes. They also provide channels for the transport of Li⁺, and buffer the volume change in charging and discharging process [32].

3.3 Electrochemical performance analysis

For PC (Fig. 4a), the broad reduction peak (0.6 V) during the initial cathodic sweep is attributed to the formation of a solid electrolyte interface (SEI) for the irreversible Li⁺ consumption [33]. The CV behavior of SnO₂/PC (Fig. 4b) is generally corresponding to those reported in literature [10, 11, 25, 34], indicating the same electrochemical reaction pathway.

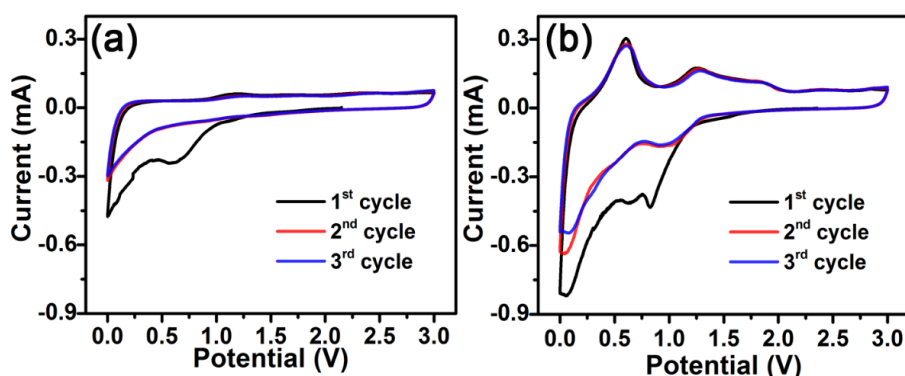


Figure 4. CV curves of PC (a) and SnO₂/PC (b) composites at 0.1 mV/s

During the first cathodic scan, three main cathodic peaks (0.85 V, 0.6 V and 0.1 V) were observed. The peak at 0.85 V represents the reduction reaction of SnO₂ with Li⁺ [1, 35]. The peak at 0.6 V manifests the formation of SEI consistent with that of PC without SnO₂. The cathodic peak at 0.1 ~ 0.25 V is about Li_xSn alloys [1, 2, 36]. In the anodic oxidation process, there are two oxidation peaks (at 0.56V, 1.26 V) for SnO₂/PC, meaning that the oxidation reaction was performed in two steps. The anodic peak at 0.56 V is the decomposing of Li_xSn. The peak at 1.26 V is ascribed to the reaction of SnO₂ and Li⁺. The CV curves indicate that SnO₂/PC and PC possesses excellent electrochemical stability.

Table 2 Comparison of SnO₂/graphene nanocomposites reported before and SnO₂/PC

Current density mA/g	Initial capacity mAh/g	Cycle number	Remaining capacity mAh/g	Ref.
50	810	30	570	[26]
55	765	100	520	[27]
67	978	30	840	[28]
264	786	50	558	[29]
100	936	100	1156	[37]
50	862	50	665	[38]
100	1499	100	1374	This work

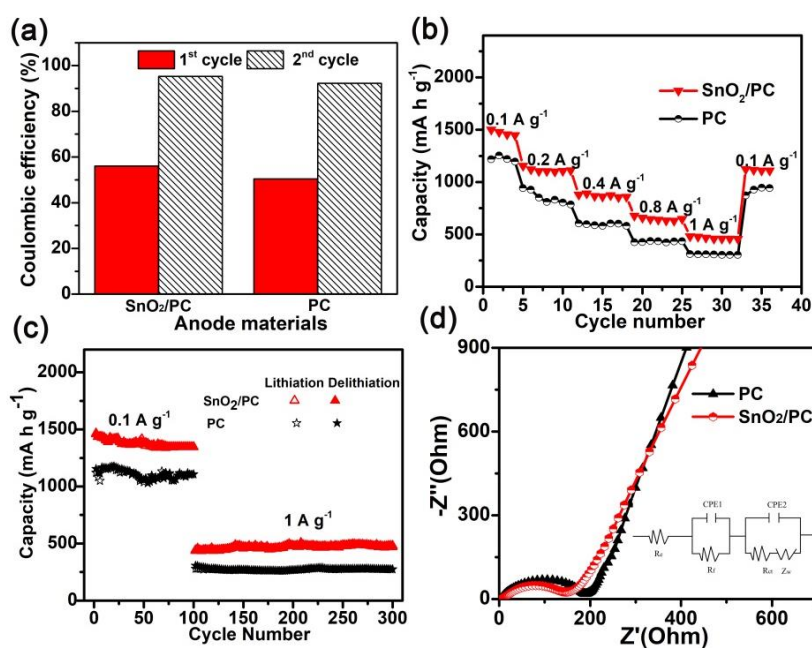


Figure 5. The coulombic efficiencies of PC and SnO₂/PC for the 1st and 2nd cycle at 0.1 A/g (a). (b) Rate capabilities of PC and SnO₂/PC. (c) Cycling performance at 0.1 A/g and 1 A/g of PC and SnO₂/PC. (d) Nyquist plots of PC and SnO₂/PC. The inset shows the equivalent circuit model.

The first coulombic efficiency for 3D SnO₂/PC (56.1%) is higher than that for 3D PC (50.4%) (Fig. 5a). The synergistic effect of 3D PC and SnO₂ nanoparticles is in favour of less irreversible Li storage. From the curves of rate capabilities (Fig. 5b), the 3D SnO₂/PC exhibits higher delithiation capacity. The delithiation capacity for 3D SnO₂/PC reaches 1499 mAh/g at 0.1 A/g and 478 mAh/g at 1 A/g, higher than that of 3D PC (1254 mAh/g at 0.1 A/g and 308 mAh/g at 1 A/g). The Li storage performance for the SnO₂/PC is also higher than currently reported value for SnO₂/GNS composites (810 mAh/g at 50 mA/g, 765 mAh/g at 55 mA/g, 978 mAh/g at 67 mA/g, 936 mAh/g at 100 mA/g) [26-28, 37]. From Fig. 5c, the 3D SnO₂/PC exhibits excellent cycling stability and the reversible specific capacity of 1374 mAh/g and 478 mAh/g at 0.1 A/g and 1 A/g is maintained after cycling. The reversible specific capacity of 1122 mAh/g at 0.1 A/g and 278 mAh/g at 1 A/g is retained for the PC anode. The reversible specific capacity of SnO₂/PC is also much higher than the value of

SnO₂/graphene hybrids reported previously (Table 2). The outstanding cycling performance might be owing to the good flexibility and structural stability. In addition, the 3D PC skeleton helps to accommodate the change of volume, and the separation and connection of SnO₂ species during discharge/charge cycles that prevents the pulverization of SnO₂ to a certain extent [26-29, 37, 38].

Fig. 5d shows the nyquist plots of PC and SnO₂/PC performed after the 300th cycle in order to further understand their electrochemical performance. The SnO₂/PC has much smaller semicircle diameter than that of the PC, manifesting that SnO₂/PC has lower charge-transfer resistance as well as contact resistance. This conclusion is consistent with previous reports [1, 15, 39]. Comparing with PC (139.0, 17.92 ohms), SnO₂/PC electrode has lower R_f and R_{ct} values (89.12, 9.87 ohms), which is enhanced by its 3D structure and ultrasmall SnO₂ nanoparticles.

4. CONCLUSIONS

In summary, 3D SnO₂/PC was successfully prepared using a simple method in this work. Benefiting from the advanced 3D hierarchical structure and ultrasmall SnO₂ nanoparticles, the nanohybrids have shown excellent electrochemical performances. At 0.1 A /g in the 100th cycle, the reversible specific capacity is 1374 mAh/g. These outstanding characteristics are desirable and make 3D SnO₂/PC a promising anode material for LIBs.

ACKNOWLEDGEMENTS

This work was supported by the National Natural Science Foundation of China (No.51702279), the Natural Science Research Project of Jiangsu Higher Education Institutions (No.18KJB430029, 19KJB480012, 19KJB430041), State Key Laboratory of Heavy Oil Processing (SKLHOP201805) and Science and Technology Planning Project of Jiangsu Province (BY2018277, BY2019195).

References

1. J. Lin, Z. Peng, C. Xiang, G. Ruan, Z. Yan, D. Natelson and J. M. Tour, *ACS Nano*, 7 (2013) 6001.
2. J. Abe, K. Takahashi, K. Kawase, Y. Kobayashi and S. Shiratori, *ACS Appl. Nano Mater.*, 1 (2018) 2982.
3. F. F. Li, G. W. Wang, D. Zheng, X. X. Zhang, C. J. Abegglen, H. N. Qu and D. Y. Qu, *ACS Appl. Mater. Interfaces*, 12 (2020) 19423.
4. Z. Wang, D. Luan, F. Y. C. Boey and X. W. Lou, *J. Am. Chem. Soc.*, 133 (2011) 4738.
5. Y. Jiang, Y. Li, P. Zhou, S. Yu, W. Sun and S. Dou, *ACS Appl. Mater. Interfaces*, 7 (2015) 26367.
6. L. Y. Ao, C. Wu, X. Wang, Y. N. Xu, K. Jiang, L. Y. Shang, Y. W. Li, J. Z. Zhang, Z. G. Hu and J. H. Chu, *ACS Appl. Mater. Interfaces*, 12 (2020) 20824.
7. J. Y. Cheong, J. H. Chang, C. Kim, J. Y. Lee, Y. S. Shim, S. J. Yoo, J. M. Yuk and I. D. Kim, *ACS Appl. Energy Mater.*, 2 (2019) 2004.
8. Y. Deng, C. Fang and G. Chen, *J. Power Sources*, 304 (2016) 81.
9. B. Chen, H. Qian, J. Xu, L. Qin, Q.-H. Wu, M. Zheng and Q. Dong, *J. Mater. Chem. A*, 2 (2014) 9345.
10. Y. N. Li, L. Zhu, T. H. Yao, T. Liu, R. F. Qian, F. Li, X. G. Han, L. M. Yu and H. K. Wang, *Energy & Fuels*, 34 (2020) 7709.
11. Y. Huang, D. Wu, J. Wang, S. Han, L. Lv, F. Zhang and X. Feng, *Small*, 10 (2014) 2226.
12. Y.-H. Hwang, E. G. Bae, K.-S. Sohn, S. Shim, X. Song, M. S. Lah and M. Pyo, *J. Power Sources*,

- 240 (2013) 683.
13. T. Ma, X. N. Yu, H. Y. Li, W. G. Zhang, X. L. Cheng, W. T. Zhu and X. P. Qiu, *Nano Letters*, 17 (2017) 3959.
 14. Z. Chen, Z. Q. Xu, W. L. Li, C. Chen, J. Yang, J. H. Liu, F. Gong, J. X. Liao and M. Q. Wu, *ACS Applied Energy Materials*, 2 (2019) 5171.
 15. D. Wang, X. Li, J. Wang, J. Yang, D. Geng, R. Li, M. Cai, T.-K. Sham and X. Sun, *The Journal of Physical Chemistry C*, 116 (2012) 22149.
 16. L.-S. Zhang, L.-Y. Jiang, H.-J. Yan, W. D. Wang, W. Wang, W.-G. Song, Y.-G. Guo and L.-J. Wan, *Journal of Materials Chemistry*, 20 (2010) 5467.
 17. X. Li, X. Meng, J. Liu, D. Geng, Y. Zhang, M. N. Banis, Y. Li, J. Yang, R. Li, X. Sun, M. Cai and M. W. Verbrugge, *Adv. Funct. Mater.*, 22 (2012) 1647.
 18. S. J. R. Prabakar, Y.-H. Hwang, E.-G. Bae, S. Shim, D. Kim, M. S. Lah, K.-S. Sohn and M. Pyo, *Adv. Mater.*, 25 (2013) 3307.
 19. D. Dixon, M. Ávila, H. Ehrenberg and A. Bhaskar, *ACS Omega*, 4 (2019) 9731.
 20. A. Vázquez-López, D. Maestre, J. Ramírez-Castellanos, J. González-Calbet, I. Píš, Silvia Nappini, N. Yuca, and A. Cremades, *The Journal of Physical Chemistry C*, 124 (2020) 18490.
 21. P. Guo, H. H. Song and X. H. Chen, *Electrochem. Commun.*, 11 (2009) 1320.
 22. F. Liu, L. Xiang and Y. Jin, *Journal of Inorganic Materials*, 19 (2004) 784.
 23. X. T. Sun, W. T. Shi, L. Xiang and W. C. Zhu, *Nanoscale Research Letters*, 3 (2008) 386.
 24. C. Cui, W. Qian, Y. Yu, C. Kong, B. Yu, L. Xiang and F. Wei, *Journal of the American Chemical Society*, 136 (2014) 2256.
 25. Y. Li, H. Zhang and P. Kang Shen, *Nano Energy*, 13 (2015) 563.
 26. S.-M. Paek, E. Yoo and I. Honma, *Nano Lett.*, 9 (2009) 72.
 27. J. Yao, X. Shen, B. Wang, H. Liu and G. Wang, *Electrochem. Commun.*, 11 (2009) 1849.
 28. X. Wang, X. Zhou, K. Yao, J. Zhang and Z. Liu, *Carbon*, 49 (2011) 133.
 29. L.-S. Zhang, L.-Y. Jiang, H.-J. Yan, W. D. Wang, W. Wang, W.-G. Song, Y.-G. Guo and L.-J. Wan, *J. Mater. Chem.*, 20 (2010) 5462.
 30. X. Wang, X. Cao, L. Bourgeois, H. Guan, S. Chen, Y. Zhong, D.-M. Tang, H. Li, T. Zhai, L. Li, Y. Bando and D. Golberg, *Adv. Funct. Mater.*, 22 (2011) 2682.
 31. J. C. Groen, L. A. A. Peffer and J. Pérez-Ramírez, *Microporous Mesoporous Mater.*, 60 (2003) 1.
 32. G. Xu, B. Ding, P. Nie, L. Shen, H. Dou and X. Zhang, *ACS Appl. Mater. Interfaces*, 6 (2014) 194.
 33. Y. Sun, G. Ning, C. Qi, J. Li, X. Ma, C. Xu, Y. Li, X. Zhang and J. Gao, *Electrochim. Acta*, 190 (2016) 141.
 34. L. Zhang, G. Zhang, H. B. Wu, L. Yu and X. W. Lou, *Adv. Mater.*, 25 (2013) 2589.
 35. B. Luo and L. Zhi, *Energy Environ. Sci.*, 8 (2015) 456.
 36. Y. Yu, L. Gu, C. Wang, A. Dhanabalan, P. A. van Aken and J. Maier, *Angew. Chem. Int. Ed. Engl.*, 48 (2009) 6485.
 37. H.H. Sheu, J.H. Syu, Y.M. Liu, K.H. Hou, M.D. Ger, *Int. J. Electrochim. Sci.*, 13 (2018) 3267.
 38. Z. Du, X. Yin, M. Zhang, Q. Hao, Y. Wang and T. Wang, *Mater. Lett.*, 64 (2010) 2076.
 39. Y. Su, S. Li, D. Wu, F. Zhang, H. Liang, P. Gao, C. Cheng and X. Feng, *ACS Nano*, 6 (2012) 8349.